INORGANIC CHEMISTRY FRONTIERS

CCS 中国化学会 CHINESE CHEMICAL SOCIETY

ROYAL SOCIETY OF CHEMISTRY

Hydrogen bonds and dispersion forces serving as molecular locks for tailored Group 11 bis(amidine) complexes

Journal:	*Inorganic Chemistry Frontiers*
Manuscript ID	QI-RES-02-2022-000443.R1
Article Type:	Research Article
Date Submitted by the Author:	10-May-2022
Complete List of Authors:	Arras, Janet; Kennesaw State University, Chemistry and Biochemistry Ugarte Trejo, Omar; Kennesaw State University, Chemistry and Biochemistry Bhuvanesh, Nattamai; Texas A&M University, McMillen, Colin; Clemson University, Department of Chemistry Stollenz, Michael; Kennesaw State University, Chemistry and Biochemistry

ARTICLE

Hydrogen bonds and dispersion forces serving as molecular locks for tailored Group 11 bis(amidine) complexes

Received 00th January 20xx,
Accepted 00th January 20xx

DOI: 10.1039/x0xx00000x

Janet Arras,[a] Omar Ugarte Trejo,[a] Nattamai Bhuvanesh,[b] Colin D. McMillen[c] and Michael Stollenz*[a]

A flexible polydentate bis(amidine) ligand **L**H_2 operates as a molecular lock for various coinage metal fragments and forms the dinuclear complexes [**L**H_2(MCl)$_2$], M = Cu (**1**), Au (**2**), the coordination polymer [{(**L**H_2)$_2$(py)$_2$(AgCl)$_3$}(py)$_3$]$_n$ (**3**), and the dimesityl-digold complex [**L**H_2(AuMes)$_2$] (**4**) by formal insertion of MR fragments (M = Cu, Ag, Au; R = Cl, Mes) into the N–H···N hydrogen bonds of **L**H_2 in yields of 43–95%. Complexes **1**, **2**, and **4** adopt C_2-symmetrical structures in the solid state featuring two interconnected 11-membered rings that are locked by two intramolecular N–H···R–M hydrogen bonds. QTAIM analyses of the computational geometry-optimized structures **1a**, **2a**, and **4a** reveal 13, 11, and 22 additional bond critical points, respectively, all of which are related to weak intramolecular attractive interactions, predominantly representing dispersion forces, contributing to the conformational stabilization of the C_2-symmetrical stereoisomers in the solid state. Variable-temperature ^{1}H NMR spectroscopy in combination with DFT calculations indicate a dynamic conformational interconversion between two C_2-symmetrical ground state structures in solution ($\Delta G_c^{\ddagger}$ = 11.1–13.8 kcal·mol^{-1}), which is accompanied by the formation of an intermediate possessing C_i symmetry that retains the hydrogen bonds.

Introduction

Hydrogen bonding represents a fundamental secondary bonding interaction in condensed phases.[1] Its essential importance for aqueous media and biological systems as well as a broad application range in catalysis, crystal engineering and the design of supramolecular structures has initially emphasized „classical" hydrogen bonds that are usually constituted by strong electronegative donor and acceptor atoms such as N and O, or halogenides. Comparably less attention has been devoted to the influence of metal centers on hydrogen bonding interactions in the ligand domain.[1c,e,2] The enhanced effect on Brønsted-Lowry acidity of water molecules through metal-ion coordination represents a well-known example for increasing the strength of a hydrogen bond donor. Less obvious but equally important is the effect of metal centers on coordinating ligands serving as hydrogen bond acceptors. These examples range from ubiquitous D–H···X–M (D = donor = N, O; X = F, Cl, Br, I) hydrogen bonds to those involving more unusual hydrogen bond acceptors such as CO or hydride.[2d] Comparative studies on D–H···X–M, D–H···X$^-$, and D–H···X–C (halocarbon) interactions in solid-state structures by Brammer et al. demonstrated that X–M acceptor groups form significantly stronger hydrogen bonds than their X–C counterparts.[2c,d] This is attributed to the increased M$^{\delta+}$–X$^{\delta-}$ bond polarity in comparison to the C–X bond. It was also found that the relative strength of D–H···X–M bonds decreases from F to I as follows: D–H···F–M >> D–H···Cl–M > D–H···Br–M > D–H···I–M. Combined NMR-spectroscopic and computational investigations by Crabtree, Eisenstein et al. on the complex series IrH_2X(PPh_3)$_2$(pyNH_2) featuring intramolecular N–H···X–Ir hydrogen bonds that are incorporated into a chelate ring confirmed this order also for the solution state (Fig. 1, left).[3]

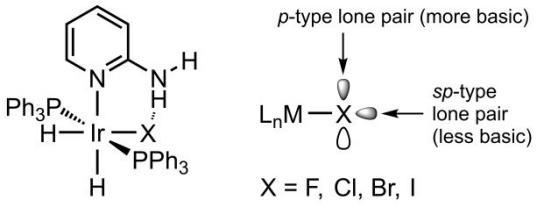

Fig. 1. Intramolecular N–H···X–M hydrogen bonds in IrH_2X(PPh_3)$_2$(pyNH_2)[3] and anisotropic preference of halides as hydrogen bond acceptors[3] at the more basic *p*-type lone pairs.

Examination of H···X–M bond angles in crystal structures showed predominantly small angles of ca. 90°–130° for Cl, Br, and I, which is consistent with a preference for halide ligands to accept protons at the more basic *p*-type lone pairs (Fig. 1, right).[2b–d] In agreement with a larger charge density but less well-defined minima of the electrostatic potential map of several examples, fluorine shows a more isotropic behavior

[a] *Department of Chemistry and Biochemistry, Kennesaw State University 370 Paulding Avenue, MD 1203, Kennesaw, Georgia 30144, USA. E-mail: Michael.Stollenz@kennesaw.edu http://facultyweb.kennesaw.edu/mstollen/*
[b] *Department of Chemistry, Texas A&M University 580 Ross Street, P.O. Box 30012, College Station, Texas 77842-3012, USA.*
[c] *Department of Chemistry, Clemson University, 379 Hunter Laboratories, Clemson, SC 29634-0973, USA.*

† Electronic Supplementary Information (ESI) available: Experimental procedures, computational details, crystallographic data and NMR spectra. CCDC 2093837 (**1**), 2093838 (**2**), and 2101719 (**3**·3(C_5H_5N)). See DOI: 10.1039/x0xx00000x

and consequently favors larger H···X–M bond angles of about 120°–160°.[2b–d]

N–H···X–M hydrogen bonding has received particular attention in Cu^{I} coordination chemistry[4] in which it has been utilized as a toolset for controlling coordination behavior[4b,e–g] and redox properties[4b,g] of Cu^{I} ions through chelate ligand design. Similar examples of Au^{I} complexes are limited[5] and Ag^{I} typically shows bridging coordination modes of ligand donor atoms or halides,[6] oftentimes resulting in polymeric arrangements[6a,c,d] (Fig. 2).

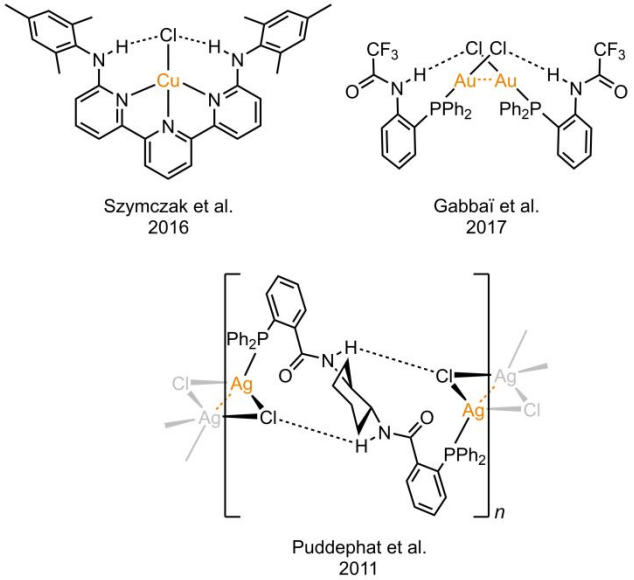

Fig. 2. Examples of N–H···Cl–M hydrogen bonds in Group 11 metal coordination spheres.[4f,5,6d]

Significantly less common are examples of D–H···R–M bonds with strong hydrogen donors in which carbon acts as acceptor atom. Generally, N–H···C and O–H···C interactions fall in the category of *non-conventional* (or *non-traditional*) hydrogen bonds that are usually weak and have been recognized in only a limited number of experimental reports as distinct bonding interactions.[7,8,9,10,11] Examples include infrared laser/microwave spectroscopic investigations on the methane-water complex,[7] the role of N–H···C bonds in organolithium chemistry,[8] solution-state and gas phase studies on carbanion[9] as well as isonitrile[10] hydrogen bonds. More current reports emphasize the role of N–H···C hydrogen bonds as modulators in luminescent *N*-heterocyclic carbene/fluorophore adducts.[11]

Very recently, we have described a dimesityl-digold bis(amidine) complex [**L**H$_2$(AuMes)$_2$] that features two rarely observed non-conventional N–H···C$_{ipso}$–Au hydrogen bonds,[12] which indicate an onset of an incipient proton transfer reaction, an important criterion for the definition of a hydrogen bond (Fig. 3).[1e] These weak hydrogen bonding interactions are supported by an ensemble of additional cooperative weak C–H···Au,[13] C–H···N, C–H···C, and C–H···H–C[14] dispersive interactions. Oftentimes being underestimated, combined dispersion forces play a key role in the stabilization of molecular structures, particularly in examples in which bulky groups have exclusively been related to steric effects.[15] Therefore, the N–H···C$_{ipso}$ hydrogen bonds in [**L**H$_2$(AuMes)$_2$] are retained in solution and instead of unfolding the double-macrocyclic double-ring structure, a conformational double-ring inversion is observed, as revealed by variable-temperature ^{1}H NMR studies and DFT calculations.

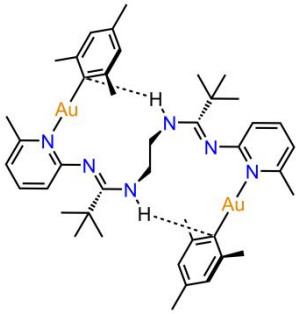

Fig. 3. Complex [**L**H$_2$(AuMes)$_2$].[12]

Originally, we became interested in alkylene-, arylene-, and dialkylsilanediyl- bridged bis(amidines) as extremely versatile ligands,[16] which have predominantly been employed in Group 1-4,[17,18,19,20] 13,[21] and 14[22] coordination chemistry, together with related catalytic studies. Applications have also included late transition metals of Groups 8-11[23,24,25,26] and the formation of multinuclear complex assemblies with more than two metal centers[17c,25,26]. Our findings revealed that these bis(amidine) ligands represent a convenient scaffold for defined linear Cu^{I} cluster arrays[27,28] that were obtained from a tetradentate bis(amidine)[29] and mesitylcopper[30].

We have earlier demonstrated that *N*,*N*'-disubstituted ethylene-bridged bis(amidines) with additional terminal *N*-donor sites exhibit unprecedented networks of weak to moderately strong inter- and intramolecular hydrogen bonds.[31] Out of this series, the hexadentate bis(amidine) **L**H$_2$ shows a C_2 symmetrical structure with two intramolecular N–H···N' hydrogen bonds that represents a tailored synthon for structurally related dinuclear complexes such as [**L**H$_2$(AuMes)$_2$]. This complex was obtained by a formal insertion of 2/5 [AuMes]$_5$ into the two N–H···N' hydrogen bonds of **L**H$_2$.

Herein, we report our findings that also coinage metal chlorides formally insert into the intramolecular NH···N hydrogen bonds of **L**H$_2$ and produce the dichloro-dicopper and –digold bis(amidine) complexes **1** and **2**, as well as the coordination polymer {[(**L**H$_2$)$_2$(py)$_2$(AgCl)$_3$](py)$_3$}$_n$ (**3**). We describe the synthesis and molecular structures of **1**–**3** that all feature assemblies of 11-membered rings constituted by intramolecular NH···Cl–M hydrogen bonds in the solid state. Moreover, an alternative synthesis of the dimesityl-digold complex [**L**H$_2$(AuMes)$_2$] (**4**) is presented by the reaction of **2** with 2 equiv. of MesMgBr. QTAIM analyses of **1**, **2**, and **4** confirm that additional cooperative weak intramolecular forces stabilize the 11-membered ring systems. Variable-temperature (VT) ^{1}H NMR spectroscopy, accompanied by a comparative computational study, reveals a concerted double-ring inversion of **1**, **2**, and **4** while retaining hydrogen bonding in solution.

Results and discussion

Synthesis, properties, and molecular structures of 1–4 in the solid state

Complexes **1** and **2** were obtained from **L**H_2 and the corresponding metal chloride precursors in THF at room temperature as colorless microcrystalline solids in excellent yields (85–95%, Scheme 1). Elemental analysis disclosed a stoichiometric composition of **L**H_2 to MCl of 1:2. This was evidenced by the characteristic $[M - Cl]^+$ fragments found in the MALDI MS spectra (see Figs. S60, S62, and S63 in the Electronic Supplementary Information, ESI). The solubility of **1** in $CDCl_3$ is decent, but poor in aromatic solvents (C_6D_6 and toluene-d_8). Although both **1** and **2** are reasonably air-stable in the solid state, solutions of **1** in $CDCl_3$, C_6D_6, and toluene-d_8 turn greenish within several hours under non-inert conditions. Complex **2** tends to degrade in $CDCl_3$ and C_6D_6 over the course of several days by forming purple solutions that are indicative of the formation of gold nanoparticles. As solids, complexes **1** and **2** are thermally stable up to 170 °C (**1**) and 180 °C (**2**) before they decompose into black oils.

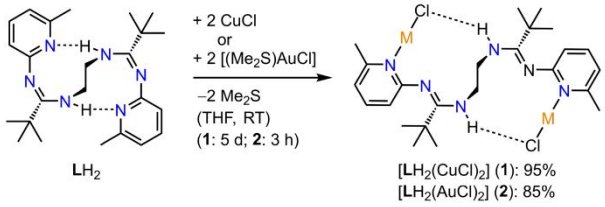

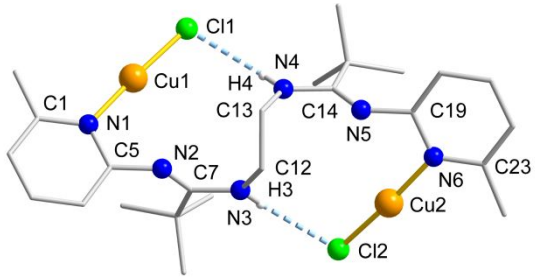

Scheme 1. Synthesis of complexes **1** and **2**. Solid-state molecular structure of **1**, determined by X-ray crystallography. Hydrogen atoms except for NH functionalities and hydrogen bonds have been omitted for clarity. Selected interatomic distances (Å), bond angles (deg), and torsion angles (deg): Cu1–Cl1 2.0961(6), Cu2–Cl2 2.1001(6), Cu1–N1 1.8934(16), Cu2–N6 1.8932(17), C12–C13 1.533(3), N3–C7 1.347(2), N2–C7 1.294(2), N4–C14 1.348(3), N5–C14 1.289(3), N1–Cu1–Cl1 175.87(5), N6–Cu2–Cl2 174.37(6), N3–C12–C13–N4 51.1(2), N1–C5–N2–C7 100.1(2), C14–N4–C13–C12 74.4(2), N6–C19–N5–C14 106.6(3). For hydrogen bonds and associated angles see Table 1 and Fig. S1, ESI.

Single crystals of **1** suitable for an X-ray structure determination were obtained from a saturated THF solution at –35 °C. This complex crystallized in the monoclinic space group $P2_1/c$ and shows four molecules occupying the unit cell (Table S1 and Fig. S3, ESI). The molecular structure of **1** shows a selective linear coordination of two CuCl fragments (N–Cu–Cl angles: 175.87(5)° and 174.37(6)°) at the terminal pyridyl moieties of the bis(amidine) ligand by formal insertion into the intramolecular N–H···N hydrogen bonds of **L**H_2 which leads to two 11-membered rings (Scheme 1). The Cu–N and Cu–Cl bonding distances (1.8934(16)/1.8932(17) Å and 2.0961(6)/2.1001(6) Å, respectively, see Figure S1, ESI) are within the range of comparable CuCl complexes with coordination number two.[32] The resulting formation of two weak to moderately strong[33] N–H···Cl–Cu hydrogen bonds is evidenced by donor-acceptor distances of 3.34-3.36 Å (Table 1), which are similar in literature examples such as a CuCl complex with a tris(pyridyl-2-methyl)amine-based ligand (3.342(2) Å, 3.366(2) Å, and 3.418(2) Å)[4b] or the example shown in Fig. 2 (3.26 and 3.353 Å, no e.s.d. given)[4f]. The N–H···Cl angles of 156–157° are clearly larger than the expected range around 90°,[2c] which is consistent with the constraints caused by the 11-membered rings consisting of the bis(amidine) ligand and the embedded CuCl fragments (Fig. S1, Table S5, ESI). The IR N–H stretching frequency of **1** is blue-shifted by 70 cm^{-1} relative to **L**H_2 and thus indicating a weaker intramolecular hydrogen bonding strength than in the free ligand (Fig. 4 and Table S4, ESI).[31]

Although the amidine binding pockets remain protonated and unoccupied, there are smaller Δ_{CN} values[34] observed for **1** (0.053/0.059 Å, Table S3, ESI) in comparison to **L**H_2 (0.056/0.069 Å)[31], which indicate a slightly increased degree of delocalization within the CN_2 amidine units.

As opposed to the free ligand **L**H_2, the bis(amidine) backbone of **1** features an *EE*(*syn*/*syn*) isomeric configuration. The (6-methyl)-pyridyl(CuCl) fragments are significantly tilted relative to the CN_2 amidine planes (by about –100 to –106°)). Complex **1** has an overall C_2 symmetry and appears as a racemic mixture in the crystalline state (Fig. S3, ESI). One enantiomer is shown in Scheme 1.

Single crystals of complex **2** were grown from a THF solution layered with diethyl ether at –35 °C and found to crystallize in the monoclinic space group *C*2/*c* with again four molecules being present in the unit cell that overall represent two pairs of C_2-symmetric enantiomers (Table S1 and Fig. S6, ESI). The molecular structure of **2** (Fig. S4, ESI) is essentially isostructural to **1**, with a notable deviation of a 4.8° larger central N–C–C–N dihedral angle and approximately 9° larger angles of the NH···Cl hydrogen bonds, which are also longer than in **1** (donor-acceptor distance: 3.389(4) Å, Table 1) and consistent with a slight blue shift of the IR N–H stretching frequency of 13 cm^{-1} relative to **1** (Fig. 4 and Table S4, ESI). This is attributed to the larger van der Waals radius of gold by 0.52 Å[35] and consequently enlarged M–Cl and M–N distances of 0.16 Å and 0.13 Å, respectively (compare Figs. S2 and S5, ESI). Similar to **1**, there is a slight deviation of the N–M–Cl angles of **2** from linearity by about 3.3° (**1**: 4.9°). The degree of delocalization in the CN_2 amidine units of **2** is about the same as in **L**H_2 (Δ_{CN} = 0.063 Å, Table S3, ESI). The Au–N (2.028(4) Å) and Au–Cl bonding distances (2.2573(11) Å, Fig. S4) are similar to those of (2-MePy)AuCl (Au–N: 2.044(4) Å; Au–Cl: 2.2590(13) Å)[36a] and [(2-(NH_2)Py)AuCl] in [(2-(NH_2)Py)$_2$Au][(2-(NH_2)Py)AuCl][$(AuCl_2]$ (Au–N: 2.053(5) Å; Au–Cl: 2.2631(9) Å)[36b].

Due to the poor solubility of AgCl in common organic solvents such as THF or acetonitrile, attempts to synthesize an analogous complex [**L**$H_2(AgCl)_2$] complex have remained unsuccessful. However, pyridine was found as a convenient solvent to generate a homogeneous solution of AgCl and **L**H_2

which allowed the isolation of complex **3** as a colorless microcrystalline solid (Scheme 2). Complex **3** is light-sensitive and starts to decompose at 139 °C. Single crystals of **3** were obtained by slow diffusion of diethyl ether into the clear reaction mixture. X-ray crystallography revealed the structure of an unusual coordination polymer $[\{(\mathbf{L}H_2)_2(py)_2(AgCl)_3\}(py)_3]_n$ that crystallized as pyridine solvate with three non-coordinating solvent molecules per monomeric unit (Scheme 2, Table S1, and Figs. S7–S9, ESI). As opposed to the linear coordination geometry in **1** and **2**, complex **3** features *two distinct* coordination modes for the MCl fragments. One AgCl unit opens an additional coordination site and interconnects two $\mathbf{L}H_2$ ligands through formal insertion into one N–H···N hydrogen bond each. In contrast to **1** and **2**, both $\mathbf{L}H_2$ bis(amidine) ligands in **3** remain in their original *ZZ*(*syn*/*syn*) isomeric configuration.[31] This gives rise to a trigonal-planar coordination environment of AgCl (N–Ag–N angle: 118.7(10)°) that is embedded in an 11-membered double ring. The terminal binding pockets of $[(\mathbf{L}H_2)_2AgCl]$ are occupied with tetrahedrally coordinated AgCl fragments which are constituted by accepting one pyridine donor molecule and dimerization to the next neighbored AgCl unit. The resulting polymeric chain is chiral and exists in only one enantiomeric form in the crystal lattice, as indicated by the monoclinic spacegroup *C*2. All coordinate bond lengths of **3** (Ag–N: 2.259(17)–2.39(3) Å; Ag–Cl: 2.494(6)–2.662(5) Å, Fig. S7, ESI) lie in the range of comparable pyridyl- and quinolyl AgCl complexes.[37] This polymeric arrangement in **3** is likely responsible for the smallest wavenumber for the IR N–H stretching modes within the series **1**–**3** and therefore its most stable N–H··· Cl–M hydrogen bonds (Table S4, ESI).

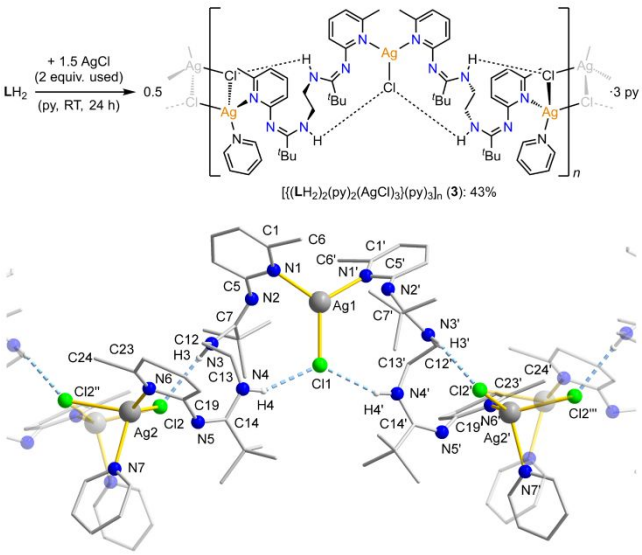

Scheme 2. Synthesis and solid-state molecular structure of complex **3**, determined by X-ray crystallography. Non-coordinating pyridine solvate molecules are not shown. Hydrogen atoms except for NH functionalities and hydrogen bonds have been omitted for clarity. Selected interatomic distances (Å), bond angles (deg), and torsion angles (deg): Ag1–Cl1 2.494(6), Ag1–N1 2.259(17), Ag2–Cl2 2.570(5), Ag2–Cl2'' 2.662(5), Ag2–N6 2.27(2), Ag2–N7 2.39(3), C12–C13 1.47(3), N3–C7 1.38(3), N2–C7 1.28(3), N4–C14 1.38(2), N5–C14 1.25(3), N1–Ag1–C11 120.6(5), N1–Ag1–N1' 118.7(10), N6–Ag2–Cl2 125.0(5), N6–Ag2–Cl2'' 118.4(7), N6–Ag2–N7 103.9(9), N7–Ag2–Cl2 114.3(7), N7–Ag2–Cl2'' 89.1(7), Cl2–Ag2–Cl2'' 100.69(17), N3–C12–C13–N4 –60(3),[38] N1–C5–N2–C7 131(2),[38] N6–C19–N5–C14 128(3)[38]. For hydrogen bonds and associated angles see Table 1 and Fig. S7, ESI.

Next, we probed the feasibility of introducing organic groups as coligands for the coinage metal ions by employing salt metathesis strategies using organolithium or Grignard reagents. This was limited to the digold complex **2**, since *σ*-organocopper and –silver bonds are more prone to protolysis by the NH functions of the amidine moieties than *σ*-aryl- and alkylgold bonds. By contrast, *σ*-organogold complexes are considerably more stable – for example, the synthesis of $[Ph_3PAuMe]$ even involves an aqueous workup step in the synthetic protocol.[39] Thus, we focused on a simple metathesis reaction of complex **2** and four equiv of MeLi, followed by hydrolysis to reestablish the NH functionalities of the bis(amidine) backbone. Since only decomposition into a purple solid (gold nanoparticles) was observed, we felt using an electronically more stabilizing and sterically encumbered group than methyl more applicable.

We have recently reported that $\mathbf{L}H_2$ and the pentameric cluster $[AuMes]_5$ cleanly convert into the dimesityl-digold complex **4**, in 95% yield (Scheme 3).[12]

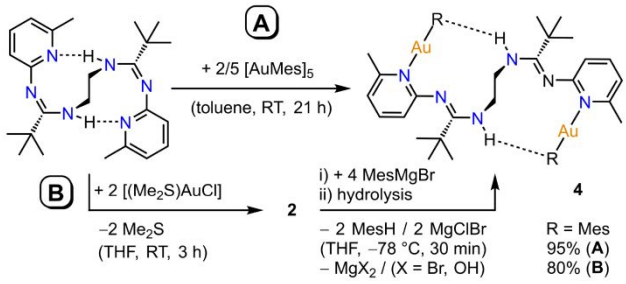

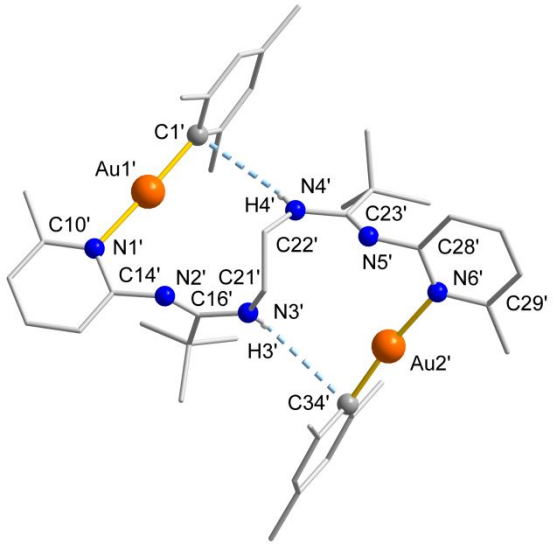

Scheme 3. Synthesis and solid-state molecular structure of complex **4**, determined by X-ray crystallography[12]. Hydrogen atoms except for NH functionalities and hydrogen bonds have been omitted for clarity. Selected interatomic distances (Å), bond angles (deg), and torsion angles (deg): Au1–C1 2.010(3), Au2–C34 2.014(3), Au1–N1 2.102(2), Au2–N6 2.111(2), C21–C22 1.518(4), N3–C16 1.350(3), N2–C16 1.289(4), N4–C23 1.354(3), N5–C23 1.290(3), N1–Au1–C1 177.4(1), N6–Au2–C34 173.35(10), N3–C21–C22–N4 56.4(3), N1–C14–N2–C16 94.0(3), N6–C28–N5–C23 84.5(4). For hydrogen bonds and associated angles see Table 1.

This synthesis was inspired by the kinetic and thermodynamic stability of mesitylgold, its excellent solubility in less polar

solvents and easy identification by only three diagnostic ^{1}H NMR signals.[40] Moreover, it has been demonstrated that mesitylgold forms mixed coinage metal clusters[41] and mononuclear mesitylgold(I) complexes with additional co-ligands[42] by rearrangements of [AuMes] fragments. We were curious about an alternative synthesis for **4**, using the dichloro-digold complex **2** and MesMgBr, because the latter is commercially available.

The reaction of **2** with four equiv of MesMgBr in THF at –78 °C, subsequent hydrolytic workup, and crystallization from CH_2Cl_2 afforded complex **4** in 80% yield (Scheme 3). The colorless microcrystals are remarkably stable and decompose around 135 °C into a dark purple oil. Complex **4** is well soluble both in $CDCl_3$ and C_6D_6. Similar to **2**, it slowly degrades in these solutions, although to a lesser extent. The stoichiometric composition of [**L**H_2(AuMes)$_2$] was confirmed by elemental analysis and the characteristic [M – Mes]$^+$ fragment in the MALDI MS spectrum. Single crystals of **4** suitable for an XRD analysis were grown as colorless blocks from a slowly concentrating diethyl ether solution at room temperature and found to crystallize in the triclinic spacegroup $P\bar{1}$. The unit cell contains one pair of C_2-symmetric enantiomers resembling the structural motif of **1** and **2**. (Scheme 3 and Ref.[12]). The two Au(I) centers show linear coordination geometries, although there is a larger deviation from linearity at Au2 (N6–Au2–C34 angle: 173.35(10)°) than at Au1 (N1–Au1–C1 angle: 177.4(1)°). This is likely due to packing effects. The Au–N bonding distances of **4** (2.102(2) Å and 2.111(2) Å) are significantly longer (by about 0.07–0.08 Å) than in **2**, which is attributed to the stronger trans influence of the mesityl ligands. Conversely, the Au–C bonds of **4** (2.010(3) Å and 2.014(3) Å) are shorter in comparison to linear gold(I)mesityl complexes with stronger trans-stabilizing co-ligands than pyridyl in **L**H_2. Those examples include phosphines in [MesAuP(Ph_2)(CH_2)$_2$(Ph_2)PAuMes] (2.067(6) Å),[40b] [MesAuP((3-Py)$_2$)(CH_2)$_2$((3-Py)$_2$)PAuMes] (2.067(4) Å),[41f] or [Ph_3PAuMes] (2.061(5) Å)[42a].

Table 1. Hydrogen bonding parameters of **L**H_2 and **1**–**4**.

	LH_2[31]	**1**	**2**[38]	**3**	**4**[12,38]
	bond/angle [Å]/[°]				
N$_{NH}$···X*	2.9461(12)	3.3583(17)	3.389(4)	3.24(2)	3.647(4)
	2.9299(12)	3.3449(17)		3.247(16)	3.525(4)
NH···X*	2.1819(9)	2.53	2.614(1)	2.44	3.04(4)
	2.2143(9)	2.52		2.46	2.86(4)
N–H···X*	140.20(7)	156.6	147.4(3)	151.3	153(4)
	138.20(7)	156.1		148.6	151(4)

*) X = Cl (**2**–**4**), X = C (**5**)

The most remarkable feature of complex **4** is its isostructural relation to **1** and **2** and the orientation of the mesityl ligands to the linking –NH(CH_2)$_2$NH– diamine bridge. This orientation initially suggested hydrogen bonding between the NH donors and the π-system of the mesityl ligands. However, a closer inspection of the structure reveals significantly shorter N···C$_{ipso}$ distances (3.525(4) Å and 3.647(4) Å) than to the next neighbored *ortho*-carbon atoms (by 0.25/0.41 Å and 0.09/0.80 Å), which indicates the existence of two *discrete* N–H···C$_{ipso}$ hydrogen bonds.

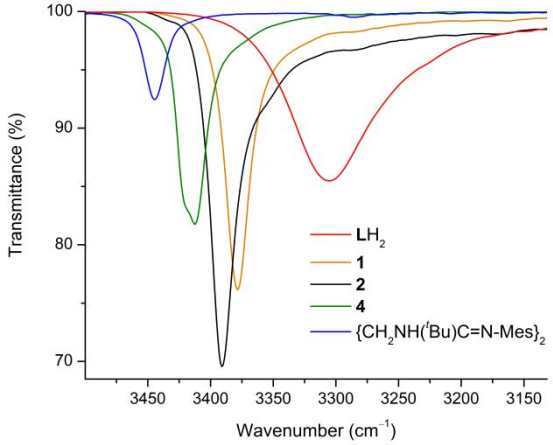

Fig. 4. NH stretching frequency region of the IR spectra of **1**, **2**, **4**[12], **L**H_2,[31] and {CH_2NH(^{t}Bu)C=N–Mes}$_2$[29].

Although the donor-acceptor distances of **4** are significantly longer (by 0.14–0.26 Å) than in **2**, the corresponding N–H···acceptor angles of **1** and **2** are within a similar range (Table 1). These parameters for **4** are consistent with a classification as weak hydrogen bonds,[33] – weaker than in **2** – which is supported by a slight blue shift of the IR N–H stretching frequency of **4** by 22 cm^{-1} in comparison to **2** (Fig. 4 and Table S4, ESI).

Quantum Theory of Atoms in Molecules (QTAIM) calculations on 1a, 2a, and 4a[12]

In the next step, we conducted quantum theory of atoms in molecules (QTAIM) analyses[43] of the computational geometry-optimized structures of **1a** and **2a** to compare the results with **4a**, focusing on the bond paths for hydrogen bonds and dispersive interactions (Table 2, Fig. 5, and Tables S15, S16, Figs. S24–S29, ESI).

Both **1a** and **2a** show bond critical points (BCPs) of the N–H···Cl hydrogen bonds with larger electronic charge densities than in **4a** ($\rho(r_{BCP})$ = 0.0192/0.0194 eÅ^{-3} for **1a**, 0.0150 eÅ^{-3} for **2a**, and 0.0081/0.0070 eÅ^{-3} for **4a**), which is expected from stronger hydrogen bonding interactions in **1a** and **2a**. This is also confirmed by larger positive Laplacians for **1a** and **2a** ($\nabla^2\rho(r_{BCP})$ = 0.0620/0.0626 eÅ^{-5} for **1a** and 0.0499 eÅ^{-5} for **2a**) relative to **4a** ($\nabla^2\rho(r_{BCP})$ = 0.0234/0.0203 eÅ^{-5}) and conclusive, because the N–H···C$_{ipso}$ hydrogen bonding interactions in **4a** have only dispersive character, consistent with electron densities found for BCPs of C≡C–H···C(π) hydrogen bonds that are in a similar range as in **4a**.[44] Consequently, the Bader charges at N (**1a**: –1.1504; **2a**: –1.1439/–1.1444) Cl (**1a**: –0.6182/–0.6176; **2a**: –0.4978/–0.4977) indicate a significantly larger polarization of the N–H···Cl bonds in **1a** and **2a** than in the N–H···C$_{ipso}$ bonds in **4a** (N: –1.1392/–1.1416 and C$_{ipso}$: –0.1632/–0.1618). In addition to the hydrogen bonds, there are 13 non-covalent bond related BCPs found in **1a**, 11 BCPs in **2a**, and 22 BCPs in **4a**. These BCPs represent distinct supporting C–

H···Au, C–H···Cl, C–H···N, C–H···C, and C–H···H–C dispersive interactions as indicated by their magnitudes of the electronic charge densities and Laplacians (Tables S15 and S16, ESI). The combination of hydrogen bonding and dispersion forces result in the extraordinary conformational stability of **1**, **2**, and **4** not only in the solid state but also in solution (*vide infra*).

Table 2. QTAIM topological parameters of selected N–H···X–M hydrogen bonds (X = Cl, C) in **1a**, **2a**, and **4a**[12]. See ESI for details.

Complex	Bond Path	Charge A	Charge B	d_{BP}(AB)	$\rho(r_{BCP})$	$\nabla^2\rho(r_{BCP})$	DI*	H	G	V
	A···B			[Å]	[eÅ^{-3}]	[eÅ^{-5}]		[Hr Å^{-3}]		
1a	N11–H12	–1.1504	0.4223	1.0134	0.3325	–1.6713	0.7110	–0.4633	0.0455	–0.5088
	H12···Cl3	0.4223	–0.6182	2.3332	0.0192	0.0620	0.0851	0.0017	0.0138	–0.0120
2a	N10···H33	–1.1439	0.4168	1.0110	0.3350	–1.6807	0.7255	–0.4657	0.0455	–0.5112
	H33···Cl3	0.4168	–0.4978	2.4454	0.0150	0.0499	0.0690	0.0019	0.0105	–0.0086
4a	N7–H8	–1.1392	0.4070	1.0075	0.3381	–1.6835	0.7462	–0.4673	0.0464	–0.5137
	H8···C11	0.4070	–0.1632	2.6359	0.0081	0.0234	0.0237	0.0011	0.0048	–0.0037

*) delocalization index

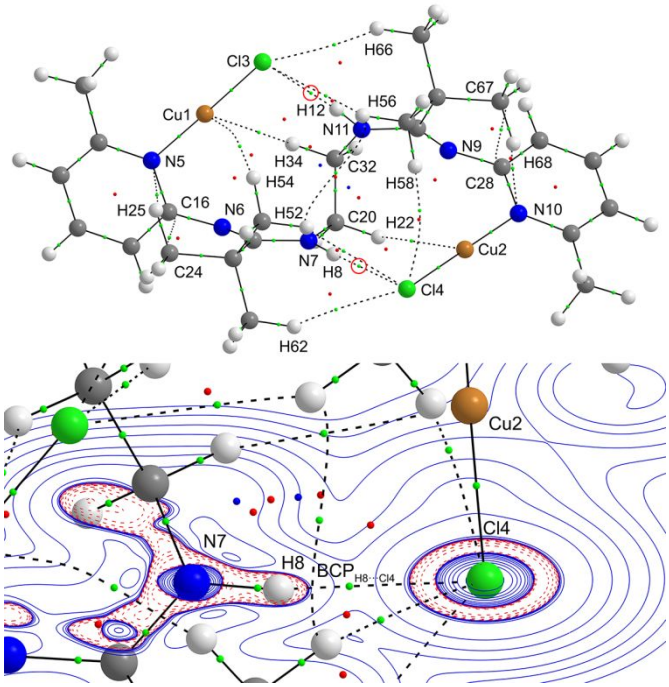

Fig. 5. Top: Atoms-in-molecules (AIM) molecular graph of **1a**. Bottom: N–H···Cl–Cu hydrogen bond region of the AIM molecular graph of **1a**. Contour map of the Laplacian of the electron density ($\nabla^2\rho(r)$) isosurfaces through the N(7)–H(8)–Cl(4) plane. Red contours show negative Laplacian ($\nabla^2\rho(r) < 0$) and blue contours show positive Laplacian ($\nabla^2\rho(r) > 0$) values. Bond critical points are denoted in green, ring critical points in red, and cage critical points in blue. See also Table 2 and ESI for more information. Geometry optimizations were performed with TURBOMOLE at the level of theory of RIDFT-D3/B3LYP/def2-TZVP. Wave functions were calculated using Gaussian at the B3LYP-D3(BJ)/6-311G(d) (for all other atoms) and the B3LYP-D3(BJ)/ECP10MDF/cc-pVTZ-PP (for Cu) level of theory. See ESI for details.

NMR spectra of 1–4 and dynamic behavior of 1, 2, and 4[12] in solution

To compare the influence of the solvent polarity on the NMR signal shifts, ^{1}H and ^{13}C{^{1}H} NMR spectra of **1**, **2**, and **4** were recorded both in $CDCl_3$ and C_6D_6. (Figs. 6, 7, and Figs. S30–S49, ESI). Due to its limited solubility in common organic solvents, pyridine-*d*[5] was used for complex **3**.

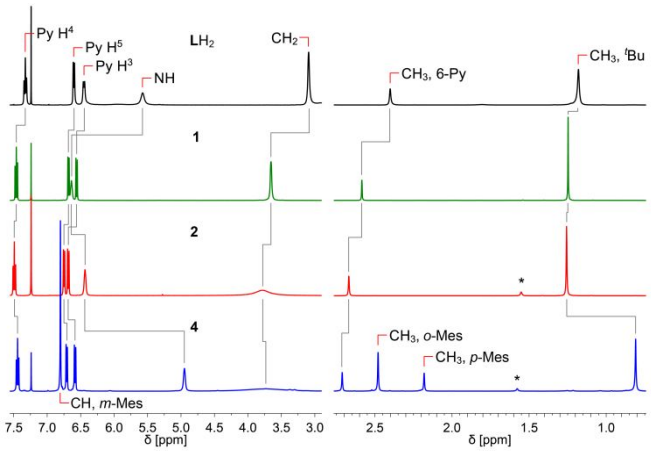

Fig. 6. Aromatic (left) and aliphatic regions (right) of ^{1}H NMR spectra of LH_2, **1**, **2**, and **4** in $CDCl_3$ (400 MHz, *) H_2O in $CDCl_3$).

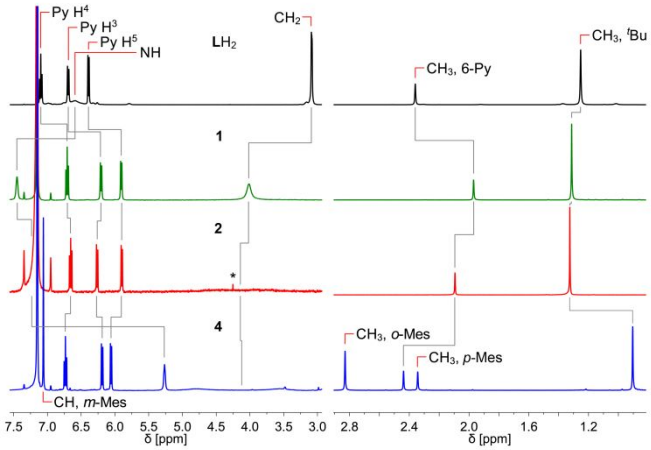

Fig. 7. Aromatic (left) and aliphatic regions (right) of ^{1}H NMR spectra of LH_2, **1**, **2**, and **4** in C_6D_6 (400 MHz, *) residual CH_2Cl_2).

All ^{1}H NMR spectra show only one set of sharp resonances for all C–H protons and thus indicate the presence of one

symmetrical stereoisomer, which implies that the unsymmetrical structure of complex **3** is not retained in solution (Table S9, ESI).

The aliphatic proton signals in **1**, **2**, and **4** are upfield-shifted by up to 1.78 ppm with respect to the free ligand **L**H_2. Notable exceptions are the 6-Py methyl group signals of **1** and **2** in C_6D_6 as well as the ^{t}Bu singlet of **4** in $CDCl_3$ and C_6D_6. A consistent trend is seen in the aromatic region for **1**, **2**, and **4**, which is electronically most affected by metal coordination. All proton signals are downfield-shifted in $CDCl_3$ ($|\Delta\delta|$ = 0.12–0.24 ppm, Py H^3; 0.11–0.16 ppm, Py H^4; and 0.08–0.15 ppm, Py H^5) and upfield-shifted in C_6D_6 ($|\Delta\delta|$ = 0.43–0.50 ppm, Py H^3; 0.37–0.45 ppm, Py H^4; and 0.20–0.49 ppm, Py H^5), relative to **L**H_2 (Table S8, ESI). The $^{13}C\{^1H\}$ NMR spectra of **1**–**4** are very similar and show the diagnostic peaks of the common bisamidine backbone essentially unchanged or with only minor relative shifts (compare Tables S10 and S11, ESI). All peaks were completely assigned by HSQC and HMBC 2D NMR experiments, with the exception of very broad or overlaid $^1H/^{13}C$ signals.

The N–H resonances of **1**, **2**, and **4** deserve particular attention, because their shifts indicate whether hydrogen bonding is retained or disrupted in the solution state. Since **L**H_2 preserves its intramolecular hydrogen bonds in solution, it does not serve as a reliable reference alone. In addition, the N–H signal in C_6D_6 is broad.[31] However, the more bulky bis(amidine) $\{CH_2NH(^tBu)C{=}N{-}Mes\}_2$ featuring the common $\{CH_2NH(^tBu)C{=}N\}$– backbone of **L**H_2 has been demonstrated to lack hydrogen bonds both in solid state and solution.[29] Although the influence of the metal fragments on the chemical shifts have to be taken into account, relative to the N–H signal of this bis(amidine), complexes **1**, **2**, and **4** show significant downfield shifts of $|\Delta\delta|$ = 0.90–2.59 ppm in $CDCl_3$ and $|\Delta\delta|$ = 1.35–2.19 ppm in C_6D_6. and thus providing strong evidence for hydrogen bonding being present in solution, which is further confirmed by VT ^1H NMR (*vide infra*). Generally, the deshielding effect of hydrogen bonds is more distinct in less polar C_6D_6 than in $CDCl_3$, because the latter also serves as a weak hydrogen bond donor/acceptor and therefore competes with the intramolecular N–H···acceptor bonds in **1**, **2**, and **4** (Tables S8 and S9, ESI). The slightly weaker downfield shifts of complex **2** compared to **1** are consistent with the structural parameters, IR data, and QTAIM computational results found for the solid state. As expected, complex **4** has the most upfield-shifted N–H resonance signals within this series, which substantiate the weak nature of the N–H···C_{ipso} hydrogen bonding interactions, although even these fragile bonds remain intact in $CDCl_3$ and C_6D_6 solutions, likely due to the additional conformational stabilization of **4** through dispersion forces.

We finally employed variable-temperature (VT) ^1H NMR spectroscopy to investigate the extraordinary conformational stability and the concerted molecular dynamics of **1**, **2**, and **4** (Figs. S50–S54, S56, and S57, ESI). While almost the entire proton signals of all three complexes remain unchanged across a wide temperature range and regardless of the solvent polarity ($CDCl_3$, C_6D_6 for **2** and **4** or CD_2Cl_2, toluene-d^7 in case of **1**), there is a remarkable change in the CH_2 region. Decreasing temperature results in increasing line broadening, followed by decoalescence, and then separation into two singlets (Fig. 8 and Figs. S50–S54, ESI).[45] Low-temperature NOESY experiments for **1** and **2** allowed the identification of two proton signals H_a and H_b through the different intensity of the H_a/NH and H_b/NH crosspeaks (Figs. S56 and S57).

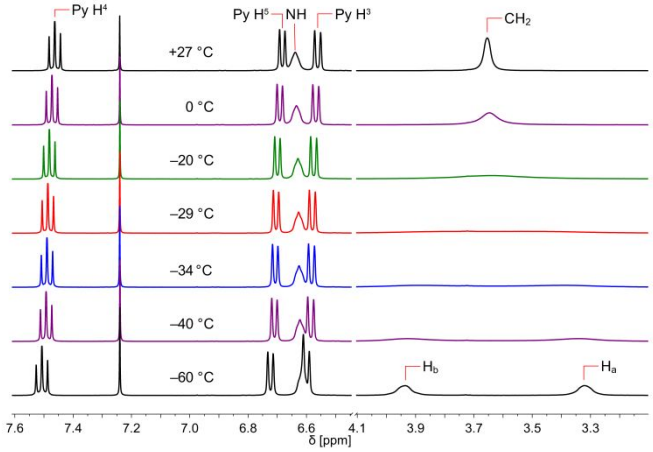

Fig. 8. Aromatic/NH region and CH_2 signals of variable-temperature ^1H NMR spectra of **1** in $CDCl_3$ (400 MHz).

In all three examples **1**, **2**, and **4** there is *no* significant shift of the N–H resonance associated with this dynamic process. Disruption of hydrogen bonding would be expected to result in an upfield-shifted N–H resonance signal.[46] This observation suggests a concerted conformational inversion of the double 11-membered ring system that retains the two N–H···acceptor hydrogen bonds and leads to a reversible interconversion from one C_2-symmetrical enantiomer into the other through the formation of a transient intermediate possessing C_i symmetry (Scheme 4).

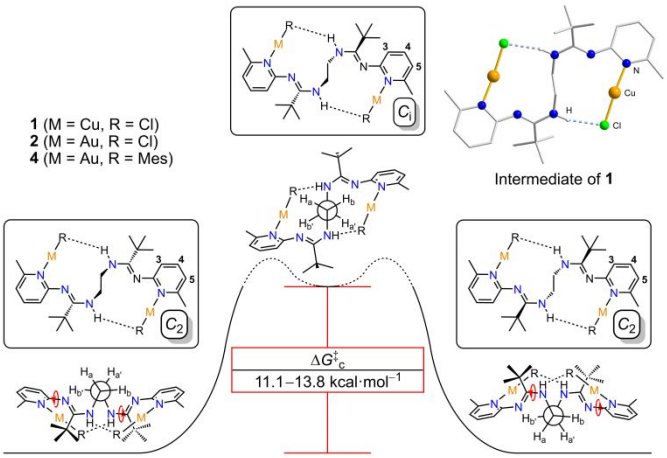

Scheme 4. Conformational double-ring inversion of **1**, **2**, and **4** in solution.[47] Computational structure of the C_i-symmetrical intermediate of **1**. Geometry optimizations were performed with TURBOMOLE at the level of theory of RIDFT-D3/B3LYP/def2-TZVP. Thermochemical corrections were calculated using Gaussian at the DFT-D3/BP-86/def2-SVP level of theory. See ESI for details.

DFT gas phase calculations suggest that the observed free energies of activation for **1**, **2**, and **4** ($\Delta G_c^{\ddagger}$ = 11.1–13.8 kcal·mol^{-1}), see also Tables 3 and S12, ESI) are in agreement with this dynamic behavior rather than a mechanism involving

disruption of hydrogen bonding. This is because the proposed C_i-symmetrical intermediates **1b**, **2b**, and **4b** are higher in free energy by ΔG = +8.0 kcal·mol^{-1} (**1b**), +13.9 kcal·mol^{-1} (**2b**), and +11.2 kcal·mol^{-1} (**4b**) than the corresponding DFT-geometry-optimized molecular structures **1a**, **2a**, and **4a**. (Table 3, Scheme 5).

Table 3. Experimental activation barrier $\Delta G_c^{\ddagger}$ of the conformational ring inversion for **1**, **2**, and **4**[12] in solution. Calculated relative free energy ΔG of **1b**, **2b**, and **3b** in the gas phase (Thermochemical corrections were calculated using Gaussian at the DFT-D3/BP-86/def2-SVP level of theory).

	1	**2**	**4**	**1b**	**2b**	**4b**
	[kcal·mol^{-1}]					
$CDCl_3$	11.1	12.9	13.0	8.0	13.9	11.2
C_6D_6	11.9*	13.5	13.8			

*) C_7D_8

Feasible alternative isomers that lack hydrogen bonds have substantially higher ΔG values, ranging from 17.2 to 23.4 kcal·mol^{-1}: **1c**, **2c**, and **4c** correspond to the C_2-symmetrical groundstate symmetry of **1a**, **2a**, and **4a**, whereas **1d**, **2d**, and **4d** have the C_i symmetry of the intermediates **1b**, **2b**, and **4b** in common. The combined VT ^{1}H NMR-spectroscopic and computational results clearly rule out an interconversion mechanism that involves separation of hydrogen bonds.

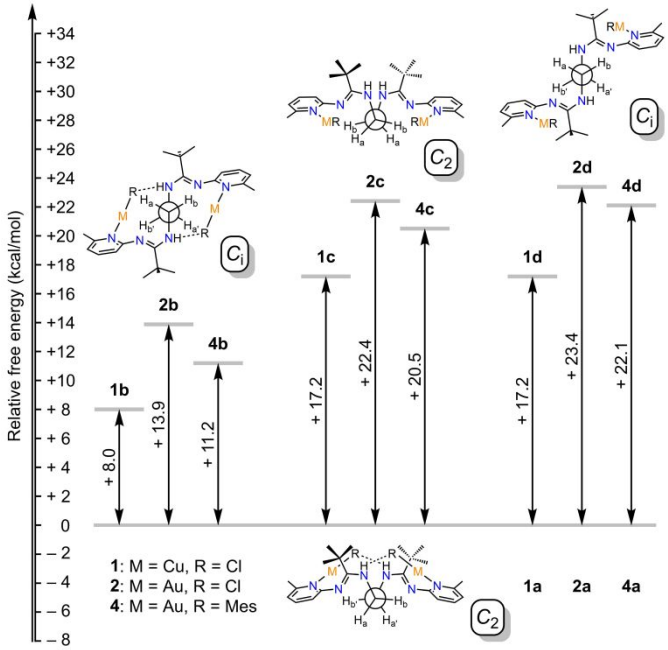

Scheme 5. Relative free energies of computationally determined isomers of **1**, **2**, and **4**[12] (**a**: geometry-optimized ground state, **b**: intermediate of the conformational ring inversion, **c** and **d**: alternative isomers without hydrogen bonds). Geometry optimizations were performed with TURBOMOLE at the level of theory of RIDFT-D3/B3LYP/def2-TZVP. Thermochemical corrections were calculated using Gaussian at the DFT-D3/BP-86/def2-SVP level of theory. See ESI for details.

Conclusions

We have demonstrated that the polydentate *N*,*N*'-disubstituted ethylene-bridged bis(amidine) **L**H$_2$ is capable of incorporating distinct CuCl, AuCl, AgCl or AuMes fragments of the [AuMes]$_5$ cluster into its pyridyl/amidine binding pockets through formal insertions of the N–H···N hydrogen bonds in **L**H$_2$. This results in the formation of the isostructural dinuclear complexes [**L**H$_2$(MCl)$_2$], M = Cu (**1**), Au (**2**), and [**L**H$_2$(AuMes)$_2$] (**4**). AgCl forms the coordination polymer [{(**L**H$_2$)$_2$(py)$_2$(AgCl)$_3$}(py)$_3$]$_n$ (**3**) in pyridine. All four examples feature N–H···acceptor hydrogen bonds, which are embedded in two flexible 11-membered interconnected rings, either found in discrete dinuclear complexes (**1**, **2**, and **4**) or arrayed in a polymeric chain (**3**). The two non-conventional N–H···C$_{ipso}$ hydrogen bonds in **4** represent rarely observed primal onsets of proton transfers in an organometallic complex. QTAIM calculations on **1**, **2**, and **4** support the existence of additional intramolecular attractive forces that predominantly include London dispersion interactions, which are altogether contribute to the overall stabilization of the C_2-symmetrical conformations of the dinuclear complexes. VT-^{1}H NMR studies of **1**, **2**, and **4** in conjunction with DFT- gas phase calculations clearly support a dynamic conformational interconversion between two C_2-symmetrical ground states rather than a mechanism that unfolds the compact complex ensemble through hydrogen bond rupture.

These findings emphasize the importance of London dispersion forces in molecular structures also showing hydrogen bonding interactions. The combination of multiple weak forces has a tremendous effect on the stabilization of energetically preferred conformations. Our example of a bulky bis(amidine) ligand framework clearly demonstrates that steric effects should always be regarded as an ensemble of steric hindrance leading to repulsion and also attraction through combined dispersion forces and hydrogen bonding. Controlling the balance of these forces by designing the molecular structure represents a new approach to manipulate supramolecular structures or reaction mechanisms, in particular those involving organometallic species in catalytic transformations.

Conflicts of interest

There are no conflicts to declare.

Acknowledgements

We thank Allan Nguyen for experimental assistance, Dr. Michael D. Walla and Dr. William E. Cotham (Mass Spectrometry Center at the University of South Carolina) for recording mass spectra, Dr. Andreas Ehnbom, Texas A&M University, for helpful discussions on computational work, and Prof. Martina Kaledin, Kennesaw State University for her help on Gaussian-related problems. Crystallographic data of complex **2** were collected through the SCrALS (Service Crystallography at Advanced Light Source) program at the Small-Crystal Crystallography Beamline 11.3.1 at the Advanced Light Source (ALS), Lawrence Berkeley National Laboratory. The ALS is supported by the U.S. Department of Energy, Office of Energy Sciences Materials Sciences Division, under contract

DE-AC02-05CH11231. The authors gratefully acknowledge support for providing computing resources by the Advanced Computer Services at Kennesaw State University. Financial support by the Department of Chemistry and Biochemistry (New Faculty Startup Fund (#08020) as well as the College of Sciences and Mathematics (CSM) at Kennesaw State University (CSM Research Stimulus Program), and by Aditya Birla Carbon (Birla Carbon Scholarship for O.U.T.) is acknowledged. This material is based upon work supported by the US National Science Foundation under Grant CHE-1800332.

Notes and references

1 (a) G. A. Jeffrey and W. Saenger, *Hydrogen Bonding in Biological Structures*, Springer, Berlin, 1991. (b) G. A. Jeffrey, *An Introduction to Hydrogen Bonding*, Oxford University Press, New York, 1997; (c) G. R. Desiraju and T. Steiner, *The Weak Hydrogen Bond in Structural Chemistry and Biology*, Oxford University Press, New York, 1999; (d) I. Alkorta, I. Rozas and J. Elguero, *Chem. Soc. Rev.*, 1998, **27**, 163–170; (e) T. Steiner, *Angew. Chem. Int. Ed.*, 2002, **41**, 48–76; (f) S. J. Grabowski, *Hydrogen Bonding - New Insights*, Springer, New York, 2006; (g) G. Gilli and P. Gilli, *The Nature of the Hydrogen Bond*, Oxford University Press, Oxford, U.K., 2009.

2 (a) G. Aullón, D. Bellamy, L. Brammer, E. A. Bruton and A. G. Orpen, Metal-bound chlorine often accepts hydrogen bonds, *Chem. Commun.*, 1998, 653–654. (b) L. Brammer, E. A. Bruton and P. Sherwood, Fluoride ligands exhibit marked departures from the hydrogen bond acceptor behavior of their heavier halogen congeners, *New J. Chem.*, 1999, **23**, 965–968 (c) L. Brammer, E. A. Bruton and P. Sherwood, Understanding the Behavior of Halogens as Hydrogen Bond Acceptors, *Cryst. Growth Des.*, 2001, **1**, 277–290. (d) L. Brammer, Metals and hydrogen bonds, *Dalton Trans.* 2003, 3145–3157.

3 E. Peris, J. C. Lee, Jr., J. R. Rambo, O. Eisenstein and R. H. Crabtree, Factors Affecting the Strength of X–H···H–M Hydrogen Bonds, *J. Am. Chem. Soc.*, 1995, **117**, 3485–3491.

4 (a) T. E. Patten, C. Troeltzsch and M. M. Olmstead, Copper(I) and -(II) Complexes of Neutral and Deprotonated *N*-(2,6-Diisopropylphenyl)-3-[bis(2-pyridylmethyl)amino]propanamide, *Inorg. Chem.* 2005, **44**, 9197–9206. (b) J. C. Mareque Rivas, S. L. Hinchley, L. Metteau and S. Parsons, The strength of hydrogen bonding to metal-bound ligands can contribute to changes in the redox behaviour of metal centres, *Dalton Trans.*, 2006, 2316–2322. (c) Z.-P. Deng, H.-L. Qi, L.-H, Huo, S. W. Ng, H. Zhao and Shan Gao, Syntheses and structures of copper(I) complexes based on Cu_nX_n (X = Br and I; n = 1, 2 and 4) units and bis(pyridyl) ligands with longer flexible spacer, *Dalton Trans.*, 2010, **39**, 10038–10050. (d) M. R. Halvagar, B. Neisen and W. B. Tolman, Copper ‐, Palladium ‐, and Platinum-Containing Complexes of an Asymmetric Dinucleating Ligand, *Inorg. Chem.* 2013, **52**, 793 ‒799. (e) S. Kumar, G. Mani, D. Dutta and S. Mishra, Structural Diversity of Copper(I) Complexes Formed by Pyrrole- and Dipyrrolylmethane-Based Diphosphine Ligands with Cu–X···HN Hydrogen Bonds, *Inorg. Chem.* 2014, **53**, 700–709. (f) E. W. Dahl and N. K. Szymczak, Hydrogen Bonds Dictate the Coordination Geometry of Copper: Characterization of a Square-Planar Copper(I) Complex, *Angew. Chem., Int. Ed.* 2016, *55*, 3101–3105. (g) E. W. Dahl, H. T. Dong and N. K. Szymczak, Phenylamino derivatives of tris(2-pyridylmethyl)amine: hydrogen-bonded peroxodicopper complexes, *Chem. Commun.*, 2018, **54**, 892–895.

5 S. Sen and F. P. Gabbaï, An ambiphilic phosphine/H-bond donor ligand and its application to the gold mediated cyclization of propargylamides, *Chem. Commun.,* 2017, **53**, 13356–13358

6 See for example: (a) G. A. Bowmaker, N. Chaichit, C. Pakawatchai, B. W. Skelton and A. H. White, Solvent-assisted mechanochemical synthesis of metal complexes, *Dalton Trans.*, 2008, 2926–2928. (b) T. S. Lobana, R. Sharma, R. J. Butcher, Synthesis, spectroscopy and structures of halogen and sulfur-bridged dinuclear silver(I) complexes with N^1-substituted thiophene-2-carbaldehyde thiosemicarbazone, *Polyhedron* 2009, **28**, 1103–1110. (c) G. A. Bowmaker, C. Pakawatchai, S. Saithong, B. W. Skelton and A. H. White, Structural and spectroscopic studies of some adducts of silver(I) halides with thiourea and *N*-ethyl substituted thioureas, *Dalton Trans.*, 2010, **39**, 4391–4404. (d) N. Nasser and R. J. Puddephatt, Self-assembled polymers of silver(I) with a chiral diphosphine ligand, *Chem. Commun.*, 2011, **47**, 2808–2810. (e) D. E. S. Silva, A. B. Becceneri, J. V. B. Santiago, J. A. Gomes Neto, J. Ellena, M. R. Cominetti, J. C. M. Pereira, M. J. Hannon and A. V. G. Netto, Silver(I) complexes of 3-methoxy-4-hydroxybenzaldehyde thiosemicarbazones and triphenylphosphine: structural, cytotoxicity, and apoptotic studies, *Dalton Trans.*, 2020, **49**, 16474–16487.

7 (a) L. Dore, R. C. Cohen, C. A. Schmuttenmaer, K. L. Busarow, M. J. Elrod, J. G. Loeser and R. J., Saykally, Far infrared vibration-rotation-tunneling spectroscopy and internal dynamics of methane-water: A prototypical hydrophobic system, *J. Chem. Phys.*, 1994, **100**, 863–876; (b) R. D. Suenram, G. T. Fraser, F. J. Lovas and Y. Kawashima, The microwave spectrum of CH_4– –H_2O, *J. Chem. Phys.*, 1994, **101**, 7230–7240.

8 (a) T. Laube, J. D. Dunitz and D. Seebach, On the Interaction between Lithium Enolates and Secondary Amines in Solution and in the Crystal, *Helv. Chim. Acta*, 1985, **68**, 1373–1393; (b) S. Buchholz; K. Harms, M. Marsch, W. Massa and G. Boche, Model of a Solvent-Shared Ion Pair with N–H···C Hydrogen Bonds between Amine and Carbanion-Crystal Structure of [Fluorenyllithium ·2 Ethylenediamine], *Angew. Chem., Int. Ed. Engl.*, 1989, **28**, 72–73; (c) S. Buchholz, K. Harms, W. Massa and G. Boche, Hydrogen Bonds between an NH_4^+ Ion and a Carbanion-Crystal Structure of Ammonium 1,2,4-Tricyanocyclopentadienide, *Angew. Chem., Int. Ed. Engl.* 1989, **28**, 73–74.

9 (a) P. Ahlberg, B. Johnsson, I. McEwen and M. Rönnqvist, Hydrogen Bonded Carbanions directly observed by ^{1}H N.M.R. and I.R. Spectroscopy, *J. Chem. Soc., Chem. Commun.*, **1986**, 1500–1501; (b) I. McEwen and P. Ahlberg, Hydrogen Bonding of a Hydroxy Proton to an lndenide Carbanion observed by N.M.R. and I.R. Spectroscopy. The Use of Cryptand to make the Alcohol Group Less Acidic than the Carbon Acid in Aprotic Solvents of Low Dielectric Constant, *J. Chem. Soc., Chem. Commun.*, **1989**, 1198–1199.

10 (a) P. v. R. Schleyer and A. Allerhand, Strong Hydrogen Bonds to Carbon in Isocyanides, *J. Am. Chem. Soc.*, 1962, **84**, 1322–1323; (b) L. L. Ferstandig, Carbon as a Hydrogen Bonding Base and Carbon-Hydrogen-Carbon Bonding, *J. Am. Chem. Soc.*, 1962, **84**, 3553–3557.

11 (a) J. A. Cowan, J. A. C. Clyburne, M. G. Davidson, R. L. W. Harris, J. A. K. Howard, P. Küpper, P., M. A. Leech and S. P. Richards, On the Interaction between N-Heterocyclic Carbenes and Organic Acids: Structural Authentication of the First N–H···C Hydrogen Bond and Remarkably Short C–H···O Interactions *Angew. Chem., Int. Ed.* 2002, **41**, 1432–1434; (b) J. M. Kieser, Z. J. Kinney, J. R. Gaffen, S. Evariste, A. M. Harrison, A. L. Rheingold and J. D. Protasiewicz, Three Ways Isolable Carbenes Can Modulate Emission of NH-Containing

Fluorophores, *J. Am. Chem. Soc.*, 2019, **141**, 12055–12063; (c) Z. J. Kinney, A. L. Rheingold and J. D. Protasiewicz, Preferential N–H/:C= hydrogen bonding involving ditopic NH-containing systems and *N*-heterocyclic carbenes, *RSC Adv.* 2020, **10**, 42164–42171.

12 J. Arras, O. Ugarte Trejo, N. Bhuvanesh and M. Stollenz, Non-conventional hydrogen bonding and dispersion forces that support embedding mesitylgold into a tailored bis(amidine) framework, *Chem. Commun.*, 2022, **58**, 1418–1421.

13 C–H···Au bonds have been substantiated only recently: (a) Md. A. Bakar, M. Sugiuchi, M. Iwasaki,; Y. Shichibu, K. Konishi, Hydrogen bonds to Au atoms in coordinated gold clusters, *Nat. Commun.*, 2017, **8**, 576. (b) M. Rigoulet, S. Massou, E. D. Sosa Carrizo, S. Mallet-Ladeira, A. Amgoune, K. Miqueu and D. Bourissou, Evidence for genuine hydrogen bonding in gold(I) complexes, *Proc. Natl. Acad. Sci. USA*, 2019, **116**, 46–51. (c) M. Straka, E. Andris, J. Vícha, A. Růžička, J. Roithová, L. Rulíšek, Spectroscopic and Computational Evidence of Intramolecular $Au^{I}\cdots H^{+}$–N Hydrogen Bonding, *Angew. Chem. Int. Ed.* 2019, **58**, 2011–2016. (d) L. Estévez, C–H···Au interactions and optical properties of $[(P,P)_4Au_6]^{2+}$ molecular gold nanoclusters, *Dalton Trans.* 2020, **49**, 4797–4804.

14 H···H bonds have been verified by QTAIM bond paths: C. F. Matta, J. Hernández-Trujillo, T.-H. Tang, R. F. W. Bader, Hydrogen – Hydrogen Bonding: A Stabilizing Interaction in Molecules and Crystals, *Chem. Eur. J.*, 2003, **9**, 1940–1951.

15 (a) J. P. Wagner and P. R. Schreiner, London Dispersion in Molecular Chemistry – Reconsidering Steric Effects, *Angew. Chem. Int. Ed.,* 2015, **54**, 12274–12296; (b) D.J. Liptrot and P. P. Power, London dispersion forces in sterically crowded inorganic and organometallic molecules, *Nat. Rev. Chem.,* 2017, **1,** 0004, 1–12;(c) T. Schnitzer, T.; E. Paenurk, N. Trapp, R. Gershoni-Poranne and H. Wennemers, Peptide–Metal Frameworks with Metal Strings Guided by Dispersion Interactions, *J. Am. Chem. Soc.*, **2021**, **143**, 644−648.

16 (a) F. T. Edelmann, Advances in the Coordination Chemistry of Amidinate and Guanidate Ligands, in *Advances in Organometallic Chemistry*, ed. A. F. Hill and M. J. Fink, Elsevier, Amsterdam, 2008, vol. 57, ch. 3, pp. 183–352. (b) R. Kretschmer, Ligands with Two Monoanionic N,N-Binding Sites: Synthesis and Coordination Chemistry, *Chem. Eur. J.* **2020**, *26*, 2099–2119.

17 Group 1: (a) G. D. Whitener, J. R. Hagadorn and J. Arnold, Synthesis and characterization of a new class of chelating bis(amidinate) ligands, *J. Chem. Soc. Dalton Trans.*, **1999**, 1249–1255. (b) R. J. Baker and C. J. Jones, Synthesis and characterisation of sterically bulky lithium amidinate and bis-amidinate complexes, *J. Organomet. Chem.*, 2006, **691**, 65–71. (c) M. S. Hill, P. B. Hitchcock and S. M. Mansell, Racemic N-aryl bis(amidines) and bis(amidinates): on the trail of enantioselective organolanthanide catalysts. *Dalton Trans.*, **2006**, 1544–1553. (d) S.-D. Bai, J.-P. Guo and D.-S. Liu, A convenient route to silyl linked bis(amidinate) ligands and synthesis of group(I) metal derivatives, *Dalton Trans.*, **2006**, 2244–2250. (e) G. G. Skvortsov, G. K. Fukin, S. Yu. Ketkov, A. V. Cherkasov, K. A. Lyssenko and A. A. Trifonov, Benzonitrile Insertion into Silylarylamides – *ansa*-Bis(benzamidinate) Ligand Systems with Rigid *o*- and *m*-Phenylene Linkers in the Synthesis of Lithium and Rare Earth Complexes, *Eur. J. Inorg. Chem.*, **2013**, 4173–4183. (f) S.-D. Bai, R.-Q. Liu, F. Guan, T. Wang, H.-B. Tong, J.-P. Guo and D.-S. Liu, Alkyl-ended *ansa*-bis(amidinate) ligands from aliphatic primary amines and multinuclear lithium derivatives, *Mendeleev Commun.*, 2013, **23**, 265–267. (g) M. Novotný, P. Švec, Z. Růžičková and A. Růžička, Direct access to non-symmetric lithium nitriloamidinate and disymmetric dilithium bisamidinate complexes from 1,3- or 1,4-dicyanobenzene and lithium amides, *J. Organomet. Chem.*, 2017, **849–850**, 88–97. (h) A. O. Tolpygin, A. V. Cherkasov, G. K. Fukin and A. A. Trifonov, Synthesis of New Bulky Bis(amidine) with the Conformationally Rigid *meta*-Phenylene Bridge and Its Dilithium Derivative $[1,3\text{-}C_6H_4\{NC(Ph)N(2,6\text{-}iso\text{-}Pr_2C_6H_3)\}_2]Li_2(TMEDA)_2$, *Russ. J. Coord. Chem.*, 2019, **45**, 235–241.

18 Group 2: A. Rösch, S. H. F. Schreiner, P. Schüler, H. Görls and R. Kretschmer, Magnesium bis(amidinate) and bis(guanidinate) complexes: impact of the ligand backbone and bridging groups on the coordination behaviour, *Dalton Trans.*, 2020, **49**, 13072–13082.

19 Group 3: see also Ref. 17. (a) S. Bambirra, A. Meetsma, B. Hessen and J. H. Teuben, Yttrium Alkyl Complex with a Linked Bis(amidinate) Ancillary Ligand, *Organometallics* 2001, **20**, 782–785. (b) J. Wang, T. Cai, Y. Yao, Y. Zhang and Q. Shen, Ytterbium amides of linked bis(amidinate): synthesis, molecular structures, and reactivity for the polymerization of L-lactide, *Dalton Trans.*, **2007**, 5275–5281. (c) J. Wang, H. Sun, Y. Yao, Y. Zhang and Q. Shen, Bridged bis(amidinate) lanthanide complexes: Synthesis, molecular structure and reactivity, *Polyhedron*, 2008, **27**, 1977–1982. (d) J. Wang, J. Li, F. Xu and Q. Shen, Anionic Bridged Bis(amidinate) Lithium Lanthanide Complexes: Efficient Bimetallic Catalysts for Mild Amidation of Aldehydes with Amines. *Adv. Synth. Catal.*, 2009, **351**, 1363–1370. (e) J. Wang, Y. Yao, Y. Zhang and Q. Shen, Bridged Bis(amidinate) Ytterbium Alkoxide and Phenoxide: Syntheses, Structures, and Their High Activity for Controlled Polymerization of L-Lactide and *ε*-Caprolactone, *Inorg. Chem.*, 2009, **48**, 744–751. (f) G. G. Skvortsov, A. O. Tolpyguin, G. K. Fukin, A. V. Cherkasov and A. A. Trifonov, Dinuclear Chlorido-, Alkyl(chlorido)-, and Hydridoyttrium Complexes Supported by μ-Bridging-Silyl-Linked Bis(amidinate) Ligands, *Eur. J. Inorg. Chem.*, **2010**, 1655–1662. (g) M. V. Yakovenko, A. V. Cherkasov, G. K. Fukin, D. Cui and A. A. Trifonov, Lanthanide Complexes Coordinated by a Dianionic Bis(amidinate) Ligand with a Rigid Naphthalene Linker, *Eur. J. Inorg. Chem.*, **2010**, 3290–3298. (h) C.-L. Pan, W. Chen, S. Su, Y.-S. Pan, J. Wang, Cubic and doubly-fused cubic samarium clusters from Sm(II)-mediated reduction of organic azides and azobenzenes, *Dalton Trans.*, 2011, **40**, 7941–7945. (i) L. Yan, H. Liu, J. Wang, Y. Zhang and Q. Shen, Divalent Lanthanide Complexes Supported by the Bridged Bis(amidinates) L [L = $Me_3SiN(Ph)CN(CH_2)_3NC(Ph)NSiMe_3$]: Synthesis, Molecular Structures and One-Electron-Transfer Reactions, *Inorg. Chem.*, 2012, **51**, 4151–4160. (j) W. Li, M. Xue, F. Xu, J. Tu, Y. Zhang and Q. Shen, Synthesis, characterization of bridged bis(amidinate) lanthanide amides and their application as catalysts for addition of amines to nitriles for monosubstituted N-arylamidines, *Dalton Trans.*, 2012, **41**, 8252–8260. (k) A. O. Tolpygin, A. S. Shavyrin, A. V. Cherkasov, G. K. Fukin and A. A. Trifonov, Chloro and Alkyl Rare-Earth Complexes Supported by *ansa*-Bis(amidinate) Ligands with a Rigid *o*-Phenylene Linker. Ligand Steric Bulk: A Means of Stabilization or Destabilization?, *Organometallics*, 2012, **31**, 5405–5413. (l) W. Li, M. Xue, J. Tu, Y. Zhang and Q. Shen, Syntheses and structures of lanthanide borohydrides supported by a bridged bis(amidinate) ligand and their high activity for controlled polymerization of ε-caprolactone, L-lactide and *rac*-lactide, *Dalton Trans.*, 2012, **41**, 7258–7265. (m) J. Tu, W. Li, M. Xue, Y. Zhang, Q. Shen, Bridged bis(amidinate) lanthanide aryloxides: syntheses, structures, and catalytic activity for addition of amines to carbodiimides, *Dalton Trans.*, 2013, **42**, 5890–5901. (n) M. Li, J. Hong, Z. Chen, X. Zhou, L. Zhang, Synthesis, structure and reactivity of dinuclear rare earth metal bis(o-aminobenzyl) complexes bearing a 1,4-phenylenediamidinate co-ligand, *Dalton Trans.*, 2013, **42**, 8288–8297. (o) A. O. Tolpygin, G. G. Skvortsov, A. V. Cherkasov, G. K. Fukin, T. A. Glukhova and A. A. Trifonov, Lanthanide Borohydrido Complexes Supported by *ansa*-Bis(amidinato) Ligands with a Rigid *o*-Phenylene Linker: Effect of Ligand Tailoring on Catalytic Lactide Polymerization. *Eur. J. Inorg. Chem.*, 2013, 6009–6018. (p) A. O. Tolpygin, A. V. Cherkasov, G.

K. Fukin and A. A. Trifonov, Reversible Switching of Coordination Mode of ansa bis(Amidinate) Ligand in Ytterbium Complexes Driven by Oxidation State of the Metal Atom. *Inorg. Chem.*, 2014, **53**, 1537−1543. (q) I. S. R. Karmel, T. Elkin, N. Fridman and M. S. Eisen, Dimethylsilyl bis(amidinate)actinide complexes: synthesis and reactivity towards oxygen containing substrates, *Dalton Trans.*, 2014, **43**, 11376–11387. (r) M. V. Yakovenko, N. Yu. Udilova, T. A. Glukhova, A. V. Cherkasov, G. K. Fukin and A. A. Trifonov, Amido rare-earth complexes supported by an *ansa* bis(amidinate) ligand with a rigid 1,8-naphthalene linker: synthesis, structures and catalytic activity in *rac*-lactide polymerization and hydrophosphonylation of carbonyl compounds, *New J. Chem.*, 2015, **39**, 1083−1093. (s) N. Kazeminejad, D. Munzel, M. D. Gamer and P. W. Roesky, Bis(amidinate) ligands in early lanthanide chemistry – synthesis, structures, and hydroamination catalysis, *Chem. Commun.*, 2017, **53**, 1060−1063. (t) G. G. Skvortsov, A. O. Tolpygin, G. K. Fukin, J. Long, J. Larionova, A. V. Cherkasov and A. A. Trifonov, Rare-Earth Complexes Coordinated by *ansa*-Bis(amidinate) Ligands with *m*-Phenylene, 2,6-Pyridinediyl, and $SiMe_2$ Linkers, *Eur. J. Inorg. Chem.*, **2017**, 4275–4284. (u) X. Yu, M. Li, J. Hong, X. Zhou and L. Zhang, Living 3,4-(Co)Polymerization of Isoprene/Myrcene and One-Pot Synthesis of a Polyisoprene Blend Catalyzed by Binuclear Rare-Earth Metal Amidinate Complexes, *Chem. Eur. J.*, 2019, **25**, 2569–2576. (v) N. Kazeminejad, L. Münzfeld, M. T. Gamer and P. W. Roesky, P. Mono- and bimetallic amidinate samarium complexes – synthesis, structure, and hydroamination catalysis, *Dalton Trans.*, 2019, **48**, 8153–8160. (w) A. O. Tolpygin, A. S. Shavyrin, A. V. Cherkasov, G. K. Fukin, I. del Rosal, L. Maron and A. A. Trifonov, Alternative (κ^1-N:η^6-arene *vs.* κ^2-N,N) coordination of a sterically demanding amidinate ligand: are size and electronic structure of the Ln ion decisive factors?, *Dalton Trans.*, 2019, **48**, 8317–8326. (x) F. Wang, X. Zhao, X. Meng and S. Wang, Rare-earth complexes supported by an ansa-bis(amidinate) ligand with a rigid *o*-phenylene linker: synthesis, structure, and catalytic activity for polymerization of cyclic esters. *Dalton Trans.*, 2019, **48**, 12193–12198.

20 Group 4: (a) J. R. Hagadorn and J. Arnold, Tethered Bis-Amidinates as Supporting Ligands: A Concerted Elimination/σ–π Rearrangement Reaction Forming an Unusual Titanium Arene Complex, *Angew. Chem. Int. Ed.*, 1998, **37**, 1729–1731. (b) J. R. Babcock, C. Incarvito, A. L. Rheingold, J. C. Fettinger and L. R. Sita, Double Heterocumulene Metathesis of Cyclic Bis(trimethylsilylamido)stannylenes and Tethered Bimetallic Bisamidinates from the Resulting α,ω-Biscarbodiimides, *Organometallics*, 1999, **18**, 5729–5732. (c) J. Hagadorn, New binucleating ligands to support dizirconium organometallics, *Chem Commun.*, **2001**, 2144–2145. (d) J. R. Hagadorn, M. J. McNevin, G. Wiedenfeld and R. Shoemaker, Dizirconium Complexes Supported by Preorganized Binucleating Bis(amidinates), *Organometallics*, 2003, **22**, 4818–4824. (e) J. Grundy, M. P. Coles and P. B. Hitchcock, Ambiphilic ligands from the 1,4-benzenebis(amidine) framework, *New J. Chem.*, 2004, **28**, 1195–1197. (f) M. J. McNevin and J. R. Hagadorn, Dititanium Complexes of Preorganized Binucleating Bis(amidinates), *Inorg. Chem.*, 2004, **43**, 8547–8554. (g) J.-F. Li, S.-P. Huang, L.-H. Weng and D.-S. Liu, Synthesis and structural studies of some titanium and zirconium complexes with chiral bis(amide), amidinate or bis(amidinate) ligands. *J. Organomet. Chem.*, 2006, **691**, 3003–3010. (h) W. Zhang and L. R. Sita, Investigation of Dynamic Intra- and Intermolecular Processes within a Tether-Length Dependent Series of Group 4 Bimetallic Initiators for Stereomodulated Degenerative Transfer Living Ziegler–Natta Propene Polymerization. *Adv. Synth. Catal.*, 2008, **350**, 439–447. (i) S.-D. Bai,; J.-P. Guo, D.-S. Liu and W.-Y. Wong, Bulky-Hindrance-Controlled Ligand Transformation from Linked Bis(amidinate) to Linked Imido-Amidinate Promoted by a Mono(cyclopentadienyl)titanium Group, *Eur. J. Inorg. Chem.*, **2006**, 4903–4907. (j) S.-D. Bai, H.-B. Tong, J.-P. Guo, M.-S. Zhou and D.-S. Liu, Coordination chemistry of group 4 metal compounds with mixed-ligand, silyl-linked bis(amidinate) ligand and cyclopentadienyl. *Inorg. Chim. Acta*, 2009, **362**, 1143–1148. (k) C.-L. Pan, W. Chen, S. Song, H. Zhang and X. Li, Stabilization of Imidosamarium(III) Cubane by Amidinates, *Inorg. Chem.*, 2009, **48**, 6344–6346. (l) S.-D. Bai, H.-B. Tong, J.-P. Guo, M.-S. Zhou, D.-S. Liu and S.-F. Yuan, Diverse coordination behaviors of the silyl-linked bis(amidinate) ligand $[SiMe_2\{NC(Ph)N(Ph)\}_2]^{2-}$ to zirconium center. *Polyhedron*, 2010, **29**, 262–269. (m) H.-B. Tong, M. Li, S.-D. Bai, S.-F. Yuan, J. B. Chao, S. Huang and D.-S. Liu, A bulky silyl shift-directed synthesis of a silyl-linked amidinate-amidine and its Zr(IV) complex, *Dalton Trans.*, 2011, **40**, 4236–4241. (n) S.-D. Bai, F. Guan, M. Hu, S.-F. Yuan, J.-P. Guo and D.-S. Liu, Mononuclear titanium compounds based on the silyl-linked bis(amidinate) ligand: synthesis, characterization and ethylene polymerization, *Dalton Trans.*, 2011, **40**, 7686–7688. (o) S.-D. Bai, R.-Q. Liu, T. Wang, F. Guan, Y.-B. Wub, J.-B. Chao, H.-B. Tong and D.-S. Liu, An alkyl-ended ansa-bis(amidine) and solvent-influenced complexation modes of its group IV metal derivatives, *Polyhedron*, 2013, **65**, 161–169. (p) T. Wang, J.-P. Zhao and S.-D. Bai, Tetrachlorido[N^2,$N^{2'}$-(dimethylsilanediyl)bis(*N*-*tert*-butyl-3-methylbenzimidamidato)-κ^2N^2,$N^{2'}$]hafnium(IV). *Acta Cryst.*, 2013, **E69**, m654.

21 Group 13: (a) H. A. Jenkins, D. Abeysekera, D. A. Dickie and J. A. C. Clyburne, Double lithiation of 2,4,6-triphenylbromobenzene: synthesis of bis-amidines and an aluminium bis-amidinate complex, *J. Chem. Soc., Dalton Trans.*, **2002**, 3919–3922. (b) J. Grundy, M. P. Coles and P. B. Hitchcock, A new class of linked-bis(*N*,*N*′-dialkylamidinate) ligand: applications in the synthesis of bimetallic aluminium complexes. *J. Organomet. Chem.*, 2002, **662**, 178–187. (c) B. Clare, N. Sarker, R. Shoemaker and J. R. Hagadorn, Synthesis and Characterization of Binucleating Bis(amidinate) Ligands and Their Dialuminum Complexes. *Inorg. Chem.*, 2004, **43**, 1159−1166. (d) Y. Lei, F. Chen, Y. Luo, P. Xu, Y. Wang and Y. Zhang, Bimetallic amidinate aluminum methyl complexes: Synthesis, crystal structure and activity for ε-caprolactone polymerization, *Inorg. Chim. Acta*, 2011, **368**, 179–186. (e) M. Bayram, D. Bläser, C. Wölper and S. Schulz, Syntheses and Structures of Bis-Amidinate−Alane Complexes. *Organometallics*, 2014, **33**, 2080−2087. (f) A. Rösch, F. Seifert, V. Vass, H. Görls and R. Kretschmer, Synthesis, structure, and catalytic activity of dinuclear aluminium bis(amidinate) and bis(guanidinate) complexes, *New. J. Chem.*, 2021, **45**, 972–981.

22 Group 14: S. Appel, F. Weller and K. Dehnicke, On the Reaction of Tin Tetrachloride with Hexakis(trimethylsilyl)-1,4-benzdiamidine. Crystal Structures of $C_6H_4[C(NSiMe_3)_2SnCl_3{\cdot}CH_3CN]_2$ and $[Na\text{-benzo-15-crown-5]}_2SnCl_6$, *Z. Anorg. Allg. Chem.*, 1990, **583**, 7–16.

23 Group 8: (a) H. Kawaguchi and T. Matsuo, Binuclear iron(II) complex from a linked-bis(amidinate) ligand: synthesis and its reaction with carbon monoxide, *Chem. Commun.*, **2002**, 958–959. (b) W.-Z. Chen and T. Ren, Symmetric and Unsymmetric "Dumbbells" of Ru_2-Alkynyl Units via C-C Bond Formation Reactions. *Inorg. Chem.*, 2006, **45**, 9175-9177.

24 Group 9: (a) E. M. B. Moos, S. González-Gallardo, M. Radius and F. Breher, Rhodium(I) Complexes of *N*-Aryl-Substituted Mono- and Bis(amidinates) Derived from Their Alkali Metal Salts. *Eur. J. Inorg. Chem.*, **2018**, 3022–3035. (b) S. Kaufmann, M. Radius, E. Moos, F. Breher and P. W. Roesky, Rhodium(I) and Iridium(I) Complexes of Ferrocenyl-Functionalized Amidinates and Bis(amidinates): κ^2N-Coordination Versus Ferrocenyl Ortho-Metalation, *Organometallics*, 2019, **38**, 1721−1732.

25 Group 10: (a) M. Ohashi, A. Yagyu, T. Yamagata and K. Mashima, Tetraplatinum precursors for supramolecular assemblies: syntheses, crystal structures, and stereoselective self-assemblies of $[Pt_4(\mu\text{-}OCOCH_3)_6(\kappa^4\text{-}N_4\text{-DArBp})]$ (DArBp = 1,3-

bis(arylbenzamidinate)propane). *Chem. Commun.*, **2007**, 3103–3105. (b) S. Tanaka, A. Yagyu, M. Kikugawa, M. Ohashi, T. Yamagata and K. Mashima, Rational Synthesis of Supramolecular Assemblies Based on Tetraplatinum Units: Synthesis, Characterization, and Selective Substitution Reactions of Four Different Pt_4 Clusters, *Chem. Eur. J.*, 2011, **17**, 3693–3709. (c) S. Tanaka and K. Mashima, Interaction of Ferrocene Moieties Across a Square Pt_4 Unit: Synthesis, Characterization, and Electrochemical Properties of Carboxylate-Bridged Bimetallic Pt_4Fe_n (n = 2, 3, and 4) Complexes, *Inorg. Chem.*, 2011, *50*, 11384–11393. (d) S. Tanaka and K. Mashima, Unique stepwise substitution reaction of a mono-(guanidinate)tetraplatinum complex with amidines, giving mono(amidinate)tetraplatinum complexes through mixed-ligand intermediate complexes. *Dalton Trans.*, 2013, **42**, 2831–2840.

26 Group 11: (a) J.-F. Liu, X. Min, J.-Y. Lv, F.-X. Pan, Q.-J. Pan and Z.-M. Sun, Ligand-Controlled Syntheses of Copper(I) Complexes with Metal−Metal Interactions: Crystal Structure and Relativistic Density Functional Theory Investigation. *Inorg. Chem.*, 2014, **53**, 11068−11074. (b) M. Dahlen, E. H. Hollesen, M. Kehry, M. T. Gamer, S. Lebedkin, D. Schooss, M. M. Kappes, W. Klopper and P. W. Roesky, Bright Luminescence in Three Phases—A Combined Synthetic, Spectroscopic and Theoretical Approach, *Angew. Chem. Int. Ed.*, 2021, **60**, 23365–23372. (c) M. Dahlen, T. P. Seifert, S. Lebedkin, M. T. Gamer, M. M. Kappes and P. W. Roesky, Tetra- and hexanuclear string complexes of the coinage metals, *Chem. Commun.*, 2021, DOI: 10.1039/d1cc06034a

27 M. Stollenz, J. E. Raymond, L. M. Pérez, J. Wiederkehr and N. Bhuvanesh, Highly Luminescent Linear Complex Arrays of up to Eight Cuprous Centers, *Chem. Eur. J.* 2016, **22**, 2396–2405.

28 M. Stollenz, Linear Copper Complex Arrays as Versatile Molecular Strings: Syntheses, Structures, Luminescence, and Magnetism, *Chem. Eur. J.* 2019, **25**, 4274–4298.

29 A. Calderón-Díaz, J. Arras, E. T. Miller, N. Bhuvanesh, C. D. McMillen and M. Stollenz, Ethylene-Bridged Tetradentate Bis(amidines): Supramolecular Assemblies through Hydrogen Bonding and Photoluminescence upon Deprotonation, *Eur. J. Org. Chem.*, 2020, **22**, 3243–3250.

30 M. Stollenz and F. Meyer, Mesitylcopper − A Powerful Tool in Synthetic Chemistry, *Organometallics* 2012, **31**, 7708–7727.

31 C. O'Dea, O. Ugarte Trejo, J. Arras, A. Ehnbom, N. Bhuvanesh and M. Stollenz, Ethylene-Bridged Hexadentate Bis(amidines) and Bis(amidinates) with Variable Binding Sites, *J. Org. Chem.*, 2019, **84**, 14217−14226.

32 See for example: (a) R. Batcup, V. T. Annibale and D. Song, Heterodinuclear complexes of 4,5-diazafluorene derivatives displaying η^5,κ^2-[N,N] and η^5,κ^1-N coordination modes, *Dalton Trans.*, 2014, **43**, 8951–8958 (Cu–N: 1.885(3)–1.890(3) Å; Cu–Cl: 2.093(1)–2.095(1) Å). (b) R. Lorenz, E. Kaifer, H. Wadepohl, H.-J. Himmel, Di- and tetranuclear transition metal complexes of a tetrakisguanidino-substituted phenazine dye by stepwise coordination, *Dalton Trans.* 2018, **47**, 11016–11029 (Cu–N: 1.910(5) Å; Cu–Cl: 2.0924(19) Å).

33 For criteria to categorize strong, moderately strong, and weak hydrogen bonds see: G. A. Jeffrey in *An Introduction to Hydrogen Bonding*, Oxford University Press, New York, 1997.

34 Δ_{CN} = *d*(C–N) – *d*(C=N) in Å; see also: G. Häfelinger and F. K. H. Kuske, General and theoretical aspects of amidines and related compounds, in *The Chemistry of Amidines and Imidates*, ed. S. Patai and Z. Rappoport, John Wiley & Sons, Ltd., Chichester, UK, 1991; pp 1−100.

35 A. Bondi, van der Waals Volumes and Radii, *J. Phys. Chem.*, 1964, **68**, 441–451.

36 (a) P. G. Jones and B. Ahrens, Gold(I) Complexes with Amine Ligands, II. Methylpyridine Complexes of Gold(I), *Z. Naturforsch., B* 1998, **53**, 653−662. (b) J. H. K. Yip, R. Feng and J. J. Vittal, $\{[AuL_2]^+[LAuCl][AuCl_2]^-\}$ (L = 2-Aminopyridine): A Trinuclear Gold(I) Unit in the Pattern [+ Neutral −]. *Inorg. Chem.*, 1999, **38**, 3586−3589.

37 Selected examples include: (a) L. M. Engelhardt, S. Gotsis, P. C. Healy, J. D. Kildea, B. W. Skelton and A. H. White, Lewis-Base Adducts of Group 11 Metal(I) Compounds. XLV Conformational Systematics of $[(N\text{-base})_1(AgX)_1]_n$ Complexes. *Aust. J. Chem.*, 1989, **42**, 149−176 (Ag–N: 2.28(3), 2.46(6) Å; Ag–Cl: 2.61(2), 2.65(4) Å). (b) C. Näther and A. Beck, Chlorotris(3-methylpyridine-*κN*)silver(I), *Acta Crystallogr.*, 2004, **E60**, m1678–1680 (Ag–N: 2.306(4) Å; Ag–Cl: 2.6066(18) Å). (c) X.-W. Dong, W. Li, H.-Y. Liu and J.-F. Ma, Di-*μ*-chloro-bis[bis(3-methylisoquinoline-*κN*)silver(I)]. *Acta Crystallogr.*, 2006, **E62**, m302–303 (Ag–N: 2.299(2), 2.306(3) Å; Ag–Cl: 2.6612(11), 2.6671(10) Å). (d) S. E. H. Etaiw and A. S. Badr El-din, Structural Influence of the Ligand Geometry on Construction of Coordination Polymers Formed from Silver(I) Chloride Ribbons and Bipodal Nitrogen Donor Ligands, *J. Inorg. Organomet. Polym.*, 2010, **20**, 684–691 (Ag–N: 2.255(3)–2.325(2) Å; Ag–Cl: 2.5151(9)–3.0281(7) Å). (e) C. Wölper, M. D. Polo Bastardés, I. Dix, D. Kratzert, and P. G. Jones, A Simple System with many Structural Variants: A Reexamination of (Amine)halogenidosilver(I) Complexes. *Z. Naturforsch. B*, 2010, **65**, 647−673 (distances in $[3,4\text{-}Me_2(C_5H_3N)AgCl]_n$, Ag–N: 2.3038(18), 2.3181(19) Å; Ag–Cl: 2.6122(7), 2.6151(6) Å).

38 These interatomic distances and torsion angles were calculated with the program DIAMOND 3.2k; the standard deviations are therefore not identical to those reported in the CIF.

39 H. Schmidbaur, A. Shiotani, Synthesis of Complex Organogold Compounds by Ligand Substitution Reactions, *Chem. Ber.*, 1971, **104**, 2821−2830.

40 (a) S. Gambarotta, C. Floriani, A. Chiesi-Villa and C. A. Guastini, Homoleptic Arylgold(I) Complex: Synthesis and Structure of Pentanuclear Mesitylgold(I). *J. Chem. Soc., Chem. Commun.*, **1983**, 1304−1305. (b) E. M. Meyer, S. Gambarotta, C. Floriani, A. Chiesi-Villa and C. A. Guastini, Polynuclear Aryl Derivatives of Group 11 Metals: Synthesis, Solid State-Solution Relationship, and Reactivity with Phosphines. *Organometallics*, 1989, **8**, 1067−1079. (c) R. Usón, A. Laguna, E. J. Fernández, M. E. Ruiz-Romero, P. G. Jones and J. Lautner, Mesitylgold(I) Complexes. Crystal Structures of $NEt_4[Au(Mes)Cl]$ and $[N(PPh_3)_2][(mes)Au(CN)Au(Mes)]$. *J. Chem. Soc., Dalton Trans.*, **1989**, 2127−2131.

41 (a) M. Contel, J. Jiménez, P. G. Jones, A. Laguna and M. Laguna, Mesitylgold Complexes: Synthesis and Reactivity; Crystal Structure of $[\{(Ph_3P)Au(\mu\text{-mes})Ag(tht)\}_2][SO_3CF_3]_2$ (mes = mesityl, tht = tetrahydrothiophene), *J. Chem. Soc., Dalton Trans.,* **1994**, 2515−2518. (b) M. Contel, J. Garrido, M. C. Gimeno, P. G. Jones, A. Laguna, M. Laguna, Trinuclear Au_2Ag and Au_2Cu Complexes with Mesityl Bridging Ligands. X-ray Structure of the Chain Polymer $[\{Au(\mu\text{-mes})AsPh_3\}_2Ag](ClO_4)$, *Organometallics*, 1996, **15**, 4939−4943. (c) M. Contel, J. Garrido, M. C. Gimeno, J. Jiménez, P. G. Jones, A. Laguna and M. Laguna, Polynuclear mesityl-gold and -gold-silver derivatives. Crystal structure of $[Ag(\mu\text{-dppm})_2\{Au(mes)\}_2]ClO_4{\cdot}3CH_2Cl_2$ (dppm = bis(diphenylphosphino) methane, mes = mesityl). *Inorg. Chim. Acta*, 1997, **254**, 157−161. (d) E. Cerrada, M. Contel, A. D. Valencia, M. Laguna, T. Gelbrich and M. B. Hursthouse, A New, Simple Route to Novel Gold Clusters: Structure of an Au Ag Wheel with a Gold Rim, *Angew. Chem. Int. Ed.*, 2000, **39**, 2353–2356. (e) E. J. Fernández, A. Laguna, J. M. López-de-Luzuriaga, M. Montiel, M. E. Olmos, J. Pérez and R. C. Puelles, Mesitylgold(I) and Silver(I) Perfluorocarboxylates as Precursors of Supramolecular Au/Ag Systems. *Organometallics*, 2006, **25**, 4307–4315. (f) M. Frik, J. Jiménez, I. Gracia, L. R. Falvello, S. Abi-Habib, K. Suriel, T. R. Muth and M. Contel, Luminescent Di- and Polynuclear Organometallic Gold(I)–Metal (Au_2, $\{Au_2Ag\}_n$ and $\{Au_2Cu\}_n$) Compounds Containing Bidentate Phosphanes as Active Antimicrobial Agents, *Chem. Eur. J.*, 2012, **18**, 3659–3674.

(g) P. Ai, C. Gourlaouen, A. A. Danopoulos and P. Braunstein, Novel Di- and Trinuclear Palladium Complexes Supported by *N*,*N*′-Diphosphanyl NHC Ligands and *N*,*N*′-Diphosphanylimidazolium Palladium, Gold, and Mixed-Metal Copper-Gold Complexes. *Inorg. Chem.*, 2016, **55**, 1219–1229.

42 (a) C. Croix, A. Balland-Longeau, H. Allouchi, M. Giorgi, A. Duchêne and J. Thibonnet, Organogold(I) complexes: Synthesis, X-ray crystal structures and aurophilicity. *J. Organomet. Chem.*, 2005, **690**, 4835–4843. (b) D. V. Partyka, J. B. Updegraff, M. Zeller, A. D. Hunter and T. G. Gray, Probing the Steric Limits of Carbon-Gold Bond Formation: (Dialkylbiarylphosphine)gold(I) Aryls. *Organometallics*, 2009, **28**, 1666–1674. (c) D. V. Partyka, M. Zeller, A. D. Hunter and T. G. Gray, Arylgold(I) Complexes from Base-Assisted Transmetalation: Structures, NMR Properties, and Density-Functional Theory Calculations. *Inorg. Chem.*, 2012, **51**, 8394−8401. (d) S. Dupuy, L. Crawford, M. Bühl,; A. M. Z. Slawin and S. P. Nolan, The Role of Metal Hydroxide Complexes in Late Transition Metal-Mediated Transmetalation Reaction: The Case of Gold. *Adv. Synth. Catal.*, 2012, **354**, 2380–2386.

43 (a) R. F. W. Bader, Atoms in Molecules: A Quantum Theory, Oxford University Press, Oxford, UK, 1990. (b) R. F. W. Bader, A Quantum Theory of Molecular Structure and Its Applications, *Chem. Rev.*, 1991, **91**, 893–928.

44 S. J. Grabowski, J. M. Ugalde, Bond Paths Show Preferable Interactions: Ab Initio and QTAIM Studies on the X–H···π Hydrogen Bond, *J. Phys. Chem. A*, 2010, **114**, 7223–7229.

45 Complex **1** and **2** show onsets of multiplets in CD_2Cl_2 at –90 °C and in $CDCl_3$ at –60 °C, respectively, that suggest geminal coupling and ^3J coupling with the NH protons (Figs. S46 and S47).

46 For earlier reports about hydrogen bonds on correlations between ^{1}H NMR chemical shifts and crystallographic data see: (a) V. Bertolasi, P. Gilli, V. Ferretti and G. Gilli, Intramolecular O–H···O hydrogen bonds assisted by resonance. Correlation between crystallographic data and ^{1}H NMR chemical shifts. *J. Chem. Soc., Perkin Trans. 2*, **1997**, 945–952. (b) T. K. Harris, Q. Zhao, and A. S. Mildvan, NMR studies of strong hydrogen bonds in enzymes and in a model compound. *J. Mol. Struct.*, 2000, **552**, 97–109.

47 Note that the transformation of C_2 to C_i results in an inversion of $H_{a'}$ to $H_{b'}$ and $H_{b'}$ to $H_{a'}$, (left entiomer to intermediate) as well as H_a to H_b and H_b to H_a, (right entiomer to intermediate), and vice versa.